ACS Synthetic Biology

pubs.acs.org/synthbio

Letter

A Cell-Free Assay for Rapid Screening of Inhibitors of hACE2-Receptor−SARS-CoV-2-Spike Binding

Nanami Kikuchi, Or Willinger, Naor Granik, Reut Gal, Noa Navon, Shanny Ackerman, Ella Samuel, Tomer Antman, Noa Katz, Sarah Goldberg, and Roee Amit*

Cite This: *ACS Synth. Biol.* 2022, 11, 1389−1396

Read Online

ACCESS | Metrics & More | Article Recommendations | Supporting Information

ABSTRACT: We present a cell-free assay for rapid screening of candidate inhibitors of protein binding, focusing on inhibition of the interaction between the SARS-CoV-2 Spike receptor binding domain (RBD) and human angiotensin-converting enzyme 2 (hACE2). The assay has two components: fluorescent polystyrene particles covalently coated with RBD, termed virion-particles (v-particles), and fluorescently labeled hACE2 (hACE2F) that binds the v-particles. When incubated with an inhibitor, v-particle−hACE2F binding is diminished, resulting in a reduction in the fluorescent signal of bound hACE2F relative to the noninhibitor control, which can be measured via flow cytometry or fluorescence microscopy. We determine the amount of RBD needed for v-particle preparation, v-particle incubation time with hACE2F, hACE2F detection limit, and specificity of v-particle binding to hACE2F. We measure the dose response of the v-particles to known inhibitors. Finally, utilizing an RNA-binding protein tdPP7 incorporated into hACE2F, we demonstrate that RNA-hACE2F granules trap v-particles effectively, providing a basis for potential RNA-hACE2F therapeutics.

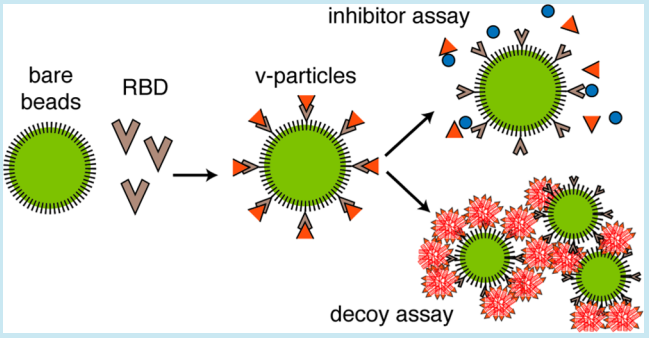

KEYWORDS: *protein−protein interaction, inhibitor, functionalized nanoparticle, drug repurposing, RNA-protein granule*

The current COVID-19 pandemic, caused by the SARS-CoV-2 virus,[1,2] has resulted in an unprecedented need for tools that combat the spread of the virus, and for therapeutics for those infected. SARS-CoV-2 virions enters the host cells via interaction between the receptor binding domain of the viral Spike protein (RBD), and hACE2 on the host cell surface.[3,4] An assay for characterization of RBD-hACE2 binding and the inhibition of this binding could be used to quantify the effect of neutralizing antibodies on the interaction of hACE2 with RBDs of emerging viral strains.[5] Furthermore, it could be used to screen candidate small molecule inhibitors of RBD-hACE2 binding, thereby accelerating the inhibitor identification step of drug discovery.[6]

Repurposing of drugs approved by either the FDA or the EMA is perhaps the fastest path for identification of approved therapeutics for emerging diseases.[7,8] *In silico* strategies are currently being employed to identify approved drugs that could be repurposed for COVID-19.[9] The standard experimental screen for candidate compounds is an *in vitro* viability assay,[10] in which *ex vivo* cells are first mixed with the compounds, and then infected with the virus. The percentage of viable cells is compared to their percentage in infected+nontreated and noninfected controls. However, high-throughput screening with cell culture requires multiple days, is relatively expensive, and requires Biosafety Level 3 biocontainment conditions. Also, assay results may differ between laboratories due to differences in cell strain, growth conditions, and inherent variability in biological response. Pseudovirus assays for SARS-CoV-2 inhibitors[11,12] require only Biosafety Level 2, but may still suffer from relatively high expense and inherent variability due to the cellular component. These constraints provide motivation for cell-free screening alternatives.[13]

Ideally, a cell-free assay for screening of inhibitors of protein−protein interaction should satisfy the following requirements: detection using standard lab equipment, repeatability, ease of use, flexibility, and low cost. Since protein sizes are well below the optical diffraction limit, some form of bulk measurement is required. To our knowledge, the only commercial cell-free option currently available for screening RBD-hACE2 inhibitors (Cayman Chemical, Cat. 502050) consists of an antibody-coated surface that binds antigen-RBD. Horseradish peroxidase (HRP)-hACE2 is introduced in the presence or absence of an inhibitor

Received: August 11, 2021
Published: April 4, 2022

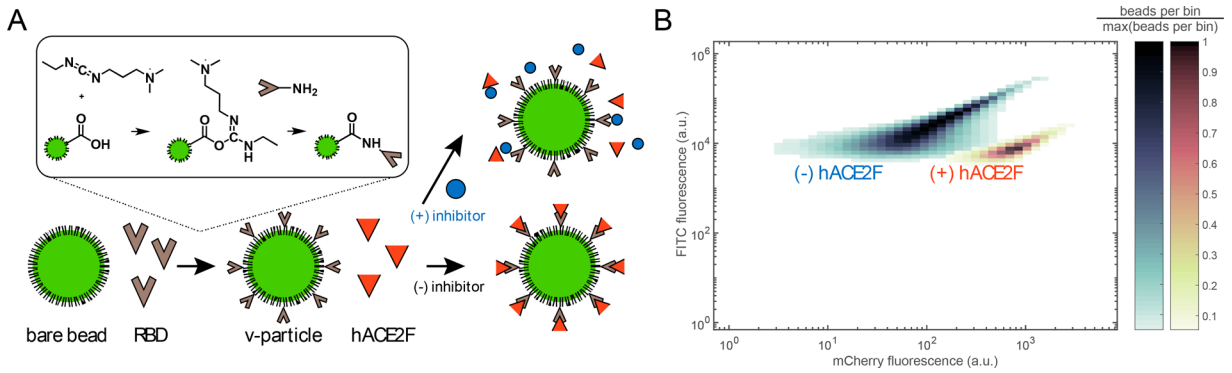

Figure 1. Schematic of the v-particle binding assay. (A) RBD is covalently attached to fluorescent polystyrene particles (green), yielding virion-like particles (v-particles). V-particles are incubated with hACE2F (red) in the presence and absence of a candidate inhibitor. (B) Experimental flow cytometry data showing v-particles in the presence (red) and absence (blue) of bound hACE2. Inhibitor activity can be quantified by the shift of the distribution to lower mCherry values.

candidate. Excess HRP-hACE2 is rinsed, and HRP activity is measured optically at 450 nm via a plate reader. However, this assay requires expensive reagents, and multiple washing steps that could affect assay repeatability. In this work, we developed a particle-based fluorescence assay for rapid screening of candidate inhibitors of RBD-hACE2 interaction without the need for live cells or viruses (see Figure 1A). Our assay utilizes a fluorescent version of hACE2 (containing mCherry, for sequence see Supplementary Table 1), which eliminates the use of antibodies and any related labeling and rinsing steps. We use fluorescent particles covalently coated with RBD, which we term v-particles, as the surface on which binding occurs. Possible roles of small particles in the context of COVID-19 have been discussed elsewhere.[14−16] In our assay, the v-particles provide a number of benefits: first, during v-particle preparation, unattached RBD can be removed from the v-particle stock via centrifugation, so that all RBD-binding events occur at the v-particle surface. This could enable production of a ready-to-use product that can be more easily shipped and stored than a coated microplate. Such a ready-to-use product could enable better quality control of the assay and yield more reproducible results.[17] Second, the v-particles provide a versatile platform: v-particles can be prepared with any choice of viral proteins (e.g., various RBD mutants) or be adapted to display any desired component without necessitating a particular chemical modification. Finally, v-particles are large enough to be easily detectable using either flow cytometry (Figure 1B) or standard fluorescence microscopy and enable clear distinction of bound hACE2 from unbound hACE2 when assayed via flow cytometer or microscope without the need for cleanup via centrifugation or buffer exchange.

RESULTS AND DISCUSSION

The RBD for the v-particles in the presented data was purchased from RayBiotech [Recombinant SARS-CoV-2, S1 Subunit Protein (RBD), cat. 230−30162]. Similar results were obtained for RBD expressed in our lab from a plasmid encoding his-tagged RBD that was a gift from the Krammer lab (see sequence in Supplementary Table S1). Lab-produced RBD[18] was extracted from HEK293F cells (Freestyle 293, Thermo Fisher) following the manufacturer's protocol (for full details, see Supplementary Methods). For v-particle generation, carboxyl fluorescent yellow particles with 0.7−0.9 μm diameter were purchased (Spherotech Inc., cat. CFP-0852-2, lot no. AM01, specified batch diameter 0.92 μm). The RBD protein was attached to the particles by two-step carbodiimide cross-linker chemistry (see Figure 1A) using *N*-(3-(dimethylamino)propyl)-N′-ethylcarbodiimide hydrochloride (EDC, Sigma-Aldrich) and *N*-hydroxysulfosuccinimide sodium salt (Sulfo-NHS, Sigma-Aldrich) (see Supplementary Methods for full details).

For the v-particle binding partner, we expressed and secreted a his-tagged fusion protein containing three domains: the extracellular domain of hACE2, the fluorescent label mCherry, and the RNA-binding protein tdPP7. While not required for the binding assay, in our hands the tdPP7 domain increased hACE2F titer relative to a fusion protein lacking the tdPP7 domain. hACE2F was expressed and secreted from HEK293F (Freestyle 293, Thermo Fisher) cells. We refer to this protein as hACE2F in the following (see Supplementary Table 1 for hACE2F sequence, and Supplementary Methods for hACE2F expression and purification).

We first optimized the concentration of the v-particle protein component using conjugation of tdPP7-mCherry instead of RBD to the carboxyl fluorescent particle, since RBD does not contain any fluorescence output (see Supplementary Table 1 for tdPP7-mCherry sequence, and Supplementary Methods for tdPP7-mCherry expression and purification). The standard curve obtained with respect to tdPP7-mCherry concentration is shown in Figure 2A. Saturation of tdPP7-mCherry is observed at 0.5x protein (x = 300 000) per bead particle (see Materials and Methods for details of component ratios). On the basis of the result for tdPP7-mCherry, we estimated that an RBD/bead molar ratio of approximately 1x would be optimal for v-particle preparation.

We next determined the working conditions for hACE2F−v-particle binding. To determine the lower limit of detection of hACE2F−v-particle binding, we measured the dependence of the mCherry fluorescence of v-particles on hACE2F concentration. The results for the sensitivity assay are shown in Figure S1A. We found that we can detect as little as ∼0.125 μg of hACE2F using 0.5 μL of v-particles in our experimental conditions, which is equivalent to a RBD/hACE2F molar ratio of 1:0.25, though a larger amount of hACE2F could provide more sensitivity when screening candidate inhibitors. We next determined the optimal time for binding reactions. On the basis of the results (Figure S1B), we determined that 15 min is sufficient for binding reactions. In this work, we decided to incubate for 45 min.

https://doi.org/10.1021/acssynbio.1c00381
ACS Synth. Biol. 2022, 11, 1389−1396

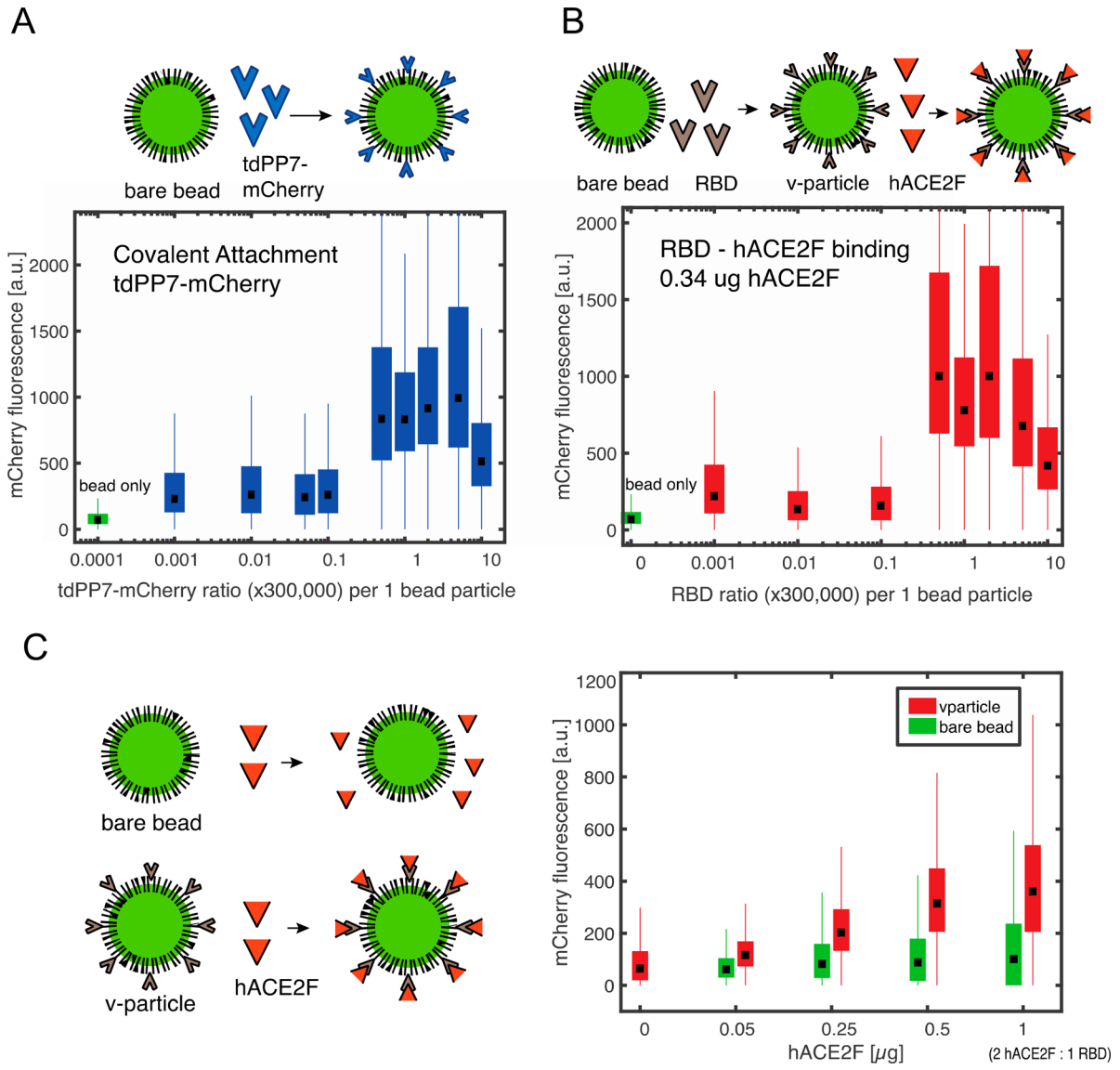

Figure 2. Optimizing v-particle synthesis and binding assay using flow cytometry. (A) Increasing amounts of tdPP7-mCherry were covalently attached to carboxyl fluorescent yellow particles (bare bead), and mCherry fluorescence of FITC-positive events was measured by flow cytometry. Schematic is indicated on top of the figure. Plateau of fluorescence indicates saturation of tdPP7-mCherry attachment onto bare bead, which is observed at 0.5 tdPP7-mCherry ratio (x300 000) per 1 bead particle (or 150 000 tdPP7-mCherry per 1 bead particle). Bead without any attachment is indicated as bead only (green). (B) 0.34 μg hACE2F was mixed with v-particles attached with increasing ratio of RBD. V-particle was synthesized using bead/RBD ratios of 1:0.001x, 1:0.01x, 1:0.1x, 1:0.5x, 1:1x, 1:2x, 1:5x, and 1:10x (x = 300 000 RBD particle). A 0.5 μL sample of those v-particles was mixed with 0.34 μg of hACE2F. Fluorescence was measured after 45 min. Schematic is indicated on top of the figure. V-particle synthesized with low amount of RBD [0.001−0.1 RBD ratio (x300 000) per 1 bead particle] or excess amount of RBD [5, 10 RBD ratio (x300 000) per 1 bead particle] shows limited or inhibited hACE2F binding, whereas v-particle with bead/RBD ratio of 1:0.5−2 (x300 000) shows optimal binding of hACE2F. Bead without any attachment is indicated as bead only (green). (C) Specificity of v-particle binding to hACE2F. Increasing amount of hACE2F was mixed with either v-particle (red) or bare bead (green). Schematic is indicated on the left of the panel. Compared to the bare bead control, a 1−2 order-of-magnitude shift in fluorescence was achieved for hACE2F mixed with v-particle at 1 μg hACE2F (2 hACE2F per one RBD), indicating hACE2F binding to the RBD displayed on the v-particles.

After determining time and useful range of hACE2F concentration, we further optimized hACE2F binding by varying the RBD/bead ratio while keeping hACE2F constant. We conjugated carboxyl particles to RBD at ratios of 1:0.001x, 1:0.01x, 1:0.1x, 1:0.5x, 1:1x, 1:2x, 1:5x, and 1:10x (x = 300 000) RBD, and added a constant amount of 0.34 μg of hACE2F. The results are shown in Figure 2B. We observe a hook effect,[19] which is typical for multicomponent binding assays: at low RBD concentration, all RBD can bind to the carboxyl particles, and hACE2F binding to v-particles is limited by the amount of conjugated RBD. The amount of conjugated RBD increases until optimal RBD/particle is reached, at which point hACE2F is also maximal. At higher RBD concentrations, not all RBD undergoes conjugation, and any remaining unconjugated RBD competes with v-particles for hACE2F binding, resulting in reduced mCherry fluorescence of v-particles. We determined that the 0.5x−2x RBD/carboxyl particle can achieve optimal mCherry fluorescence. Therefore, the final molecular ratio is around 1x RBD per 1 carboxyl bead.

https://doi.org/10.1021/acssynbio.1c00381
ACS Synth. Biol. 2022, 11, 1389−1396

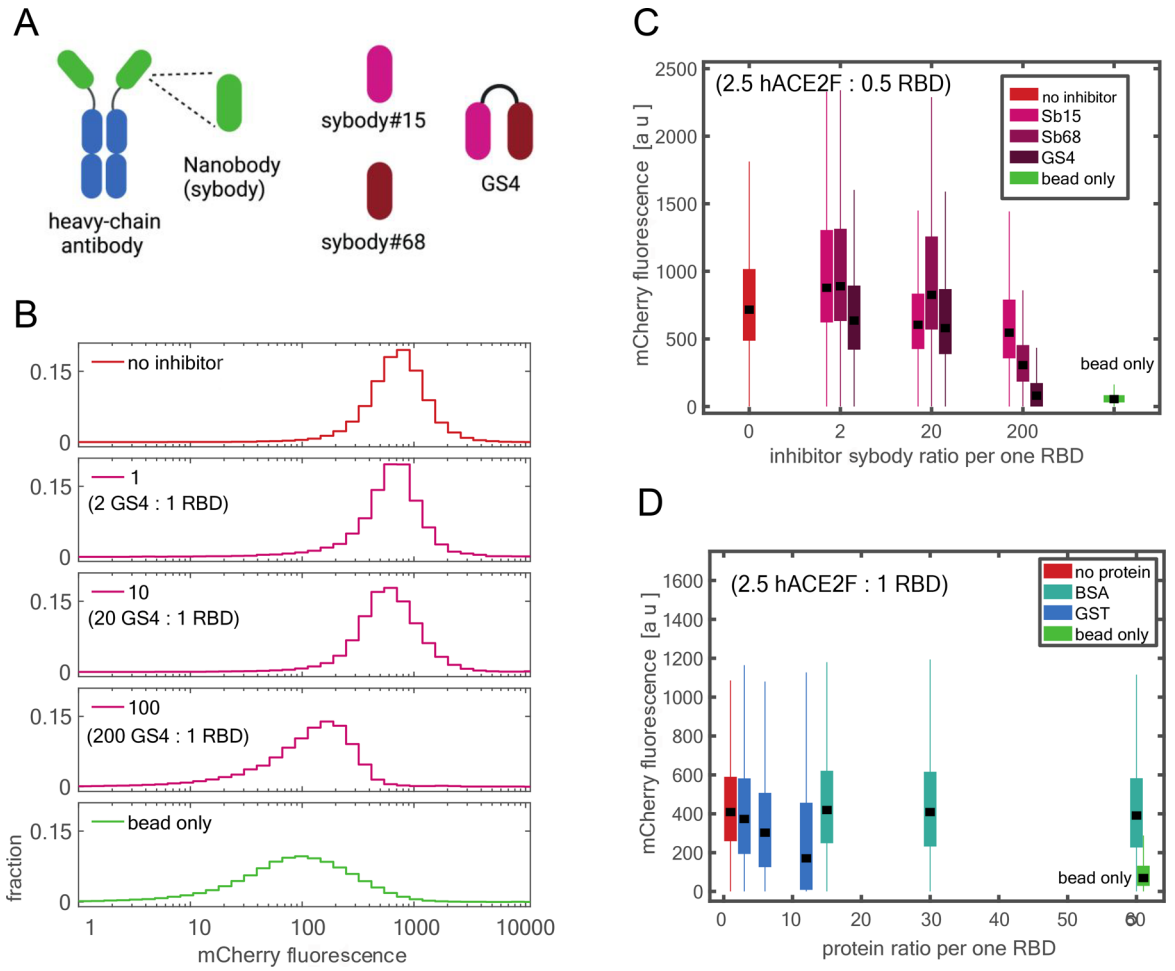

Figure 3. Inhibition of v-particle−hACE2F binding by sybodies Sb#15, Sb#68, and GS4. (A) Sybodies Sb#15 (Sb15), Sy#68 (Sb68), and a fusion of Sb15 and Sb68 (GS4), were prepared and used in the assay. (B) Flow cytometry data for GS4. Top histogram shows fluorescence associated with no inhibitor, corresponding to maximum fluorescence. Bottom histogram shows fluorescence associated with bead only, or fluorescence noise level. Fluorescence peak shifts from high fluorescence to low fluorescence as the amount of GS4 (shown as a molecular ratio of GS4 to RBD) is increased. (C) Flow cytometry data obtained from v-particle−hACE2F inhibition by Sb#15, Sb#68, and GS4. Fluorescence associated with no inhibitor is indicated in red. Fluorescence associated with bead only is indicated in green. The molecular ratio of three components hACE2F, RBD, and inhibitor is indicated. (D) Flow cytometry data obtained from v-particle−hACE2F inhibition by control proteins BSA and GST. Fluorescence associated with no protein indicated in red. Fluorescence associated with bead only indicated in green. The molecular ratio of three component, hACE2F, RBD, and protein is indicated. Note that commercial BSA and GST buffer components (e.g., glycerol) may have interfered with the assay.

We next verified the specificity of v-particle binding to hACE2F by comparing to carboxyl fluorescent yellow particle (bare bead) binding to hACE2F (Figure 2C). The plot shows that v-particles incubated with comparable amounts of hACE2F exhibit a modest and continuous concentration-dependent shift (red) in mCherry fluorescence, compared to the shift seen for bare bead (green), which is consistent with nonspecific binding. This indicates specific binding of hACE2F to the RBD displayed on the v-particles.

As a proof-of-concept for inhibitor screening, we measured the inhibition of v-particle−hACE2F binding in the presence and absence of synthetic peptide inhibitors, or sybodies, Sb#15, Sb#68, and GS4[20] (Figure 3A). For details of sybody expression see Supplementary Methods. For comparison, we measure v-particle−hACE2F binding in the absence of inhibitor, and the fluorescence of the bare-bead control. We observe a shift in fluorescence with increasing sybody concentration, indicating a reduction in v-particle−hACE2F binding. For GS4 particularly, we see a dose-dependent reduction in the fluorescence distribution. We plot the histogram of the v-particle mCherry fluorescence as a function of the GS4 dose (Figure 3B), which provides a quantitative assay of RBD-hACE2F inhibition. The flow cytometry results for the three inhibitor sybodies are plotted in Figure 3C. For comparison, we tested bovine serum albumin (BSA, New England Biolabs) and glutathione S-transferase (GST, Sigma-Aldrich cat. SRP5348), which are not known to inhibit RBD-hACE2F binding (Figure 3D). We note that GST stock concentration was low, and thus any inhibition that might be inferred may be due to the increased buffer components in the binding assay for this protein, and not to the protein itself.

Finally, we utilized the v-particles to assess the efficacy of synthetic RNA-protein (SRNP) granules in binding to, and thereby depleting the active amount of, SARS-CoV-2 virions. Here, the v-particles provide a safe and microscopically visible alternative to actual virions. RNA-protein granules can be produced *in vitro*,[21,22] and have been shown to bind cellular components.[22,23] We recently showed[24] that SRNP granules form specifically *in vitro* via self-assembly by mixing purified bacterial phage coat proteins with synthetic long noncoding

https://doi.org/10.1021/acssynbio.1c00381
ACS Synth. Biol. 2022, 11, 1389−1396

RNA (slncRNA) molecules that encode multiple binding sites for the coat proteins. In this case, the protein component in the granule formulation was either tdPP7-mCherry, or hACE2F (see Supplementary Methods and Supplementary Table 1 for both proteins). The slncRNA component (slncRNA-PP7bsx14, see Supplementary Table 1 for sequence and Supplementary Methods for synthesis details) harbors 14 PP7 binding sites, to which the tdPP7 domain present in both hACE2F and tdPP7-mCherry can bind. The RNA thus increases the local concentration of hACE2F, which may facilitate virion entrapment and thus potentially function as an anti-SARS-CoV-2 decoy particle (Figure 4A). To test for selective binding of the SRNP granules to the v-particles, we prepared the following samples: v-particles with slncRNA-PP7bsx14 and tdPP7-mCherry, v-particles with hACE2F, and v-particles with slncRNA-PP7bsx14 and hACE2F. We show the results of the binding experiments in Figure 4. In the microscopy images, v-particles appear as green fluorescent beads (Figure 4B). SRNP-granules appear as large red clumps or as bead-like particles (Figure 4C), which are located on the coverslip at different positions from the v-particles. When v-particles are mixed with hACE2F, colocalization of the hACE2F protein to the v-particles is observed, as expected from our previous experiments (Figure 4D). Finally, hACE2F-SRNP-granules appear to be bound to the v-particles (Figure 4E and Figure S2), as compared with the non-hACE2F-SRNP-granules which appear to be spatially separated from the v-particles (Figure 4C). Consequently, the SRNP-hACE2F granules provide a potential decoy or anti-SARS-CoV-2 therapeutic, which should be examined in follow-up research.

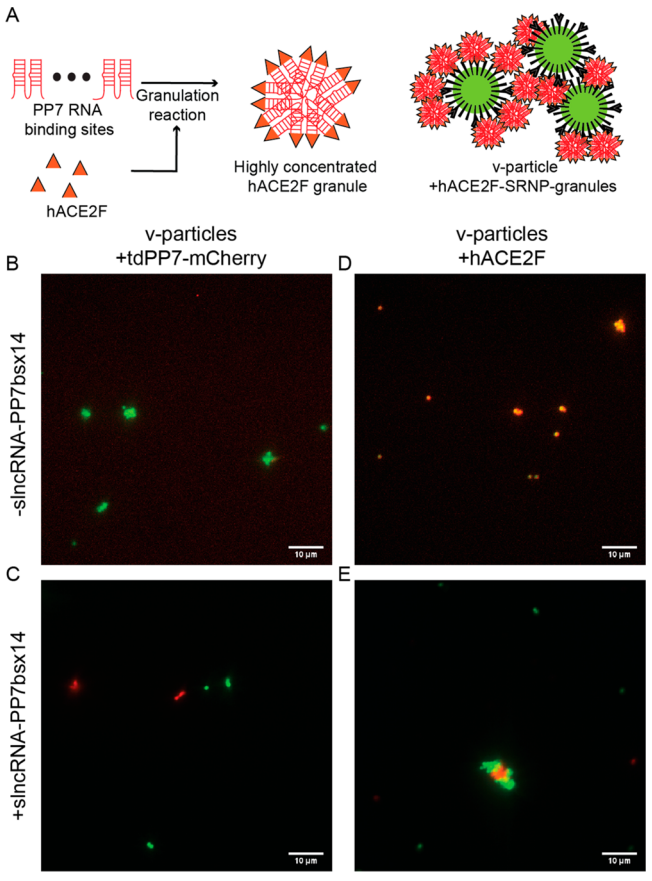

Figure 4. Entrapment of v-particles by slncRNA-PP7bsx14 - hACE2F granules. (A) Schematic of the hACE2F SRNP granules sequestration assay. (Left) RNA containing PP7 binding sites is incubated with hACE2F proteins to form SRNP granules with high protein concentration. (Right) SRNP granules attach to the v-particles via hACE2-RBD binding, serving as decoys. (B–E) Overlay of fluorescence microscopy images at 585 nm (mCherry) and 490 nm (FITC) excitation wavelengths. (B) V-particles incubated with tdPP7-mCherry, (C) v-particles incubated with slncRNA-PP7bsx14 - tdPP7-mCherry granules, (D) v-particles incubated with hACE2F, and (E) v-particles incubated with slncRNA-PP7bsx14 - hACE2F granules. For (A–E), v-particle concentration was 0.1% w/v. Protein concentrations in imaged samples were (B,C) 842 nM, (D) 560 nM, and (E) 507 nM. slncRNA-PP7bsx14 concentration in imaged samples was 112.8 nM (C,E).

We have presented a particle-based assay that enables rapid, cell-free screening of candidate inhibitors of protein–protein interaction, focusing on the interaction between SARS-CoV-2 Spike RBD bound to fluorescent particles (v-particles), and fluorescently tagged hACE2 (hACE2F). The assay materials are commercially available or relatively easy to prepare and do not include antibody components. The main difficulty in assay preparation is the production of the protein components. Depending on available lab resources, researchers may choose to outsource this step. We demonstrated the utility of the assay for quantifying inhibition of RBD–hACE2 interaction by the reported inhibitor GS4, Sb#15, and Sb#68 as well as with a potential anti-SARS-CoV-2 RNP–granule decoy particle. Although we described applications specific to RBD and hACE2F interaction, the presented applications could easily be modified to quantify interaction of other peptide–receptor interaction partners, such as RBD mutants with either hACE2 or other suspected host receptors,[25] or other viral proteins with their respective host partners.[26] We further demonstrated that v-particles can provide a cell-free alternative to more expensive and higher-biosafety-level cell-based assays for assessing proposed SARS-CoV-2 entrapment products. We hope that the relatively straightforward preparation, ease of use, and quantitative results of our v-particles and binding assay will have a significant impact in assays involving SARS-CoV-2 variants, as well as other viruses.

MATERIALS AND METHODS

Details of protein expression and purification for his-tagged RBD, hACE2F, tdPP7-mCherry, and sybodies Sb#15, Sb#68, and GS4 appear in the Supporting Information. Details of slncRNA-PP7bsx14 preparation appear in the Supporting Information. Details of v-particle preparation appear in the Supporting Information. Calculation of all component ratios appears in the Supporting Information.

Flow-Cytometry Binding Assays. V-particles and protein components were added according to the details below. BSA (20 mg/mL, New England Biolabs) was added at a ratio of 10 μg of BSA per 0.5 μL of v-particle stock (1 μL v-particle = 2.2 × 10^7 bead particles. According to the manufacturer one bead particle contains up to 300 000 COOH functional groups, 0.5 μL of v-particles contains up to 0.6 × 10^{-11} mol RBD or 3.6× 10^{12} RBD single protein molecules) to all binding reactions to suppress nonspecific binding of protein to the v-particles. Unless stated otherwise, samples were incubated on ice for 45 min. All sample volumes were adjusted to 100 μL with 1x PBS and measured via flow cytometry (MACSquant VYB, Miltenyi Biotec). The flow cytometer was calibrated using MacsQuant calibration beads (Miltenyi Biotec) before measurement, and 0.5 μL of 1% w/v amine polystyrene fluorescent yellow

https://doi.org/10.1021/acssynbio.1c00381
ACS Synth. Biol. 2022, 11, 1389–1396

particles (Spherotech, Inc., cat. AFP-0852-2, lot No. V01-R) or carboxyl polystyrene fluorescent yellow particles in 100 μL of 1x PBS were run as a negative control. Negative controls behaved similarly. Voltages for the SSC, FSC, FITC (B1), and mCherry (Y2) channels were 400, 200, 325, and 300 V, respectively. Events were defined using an FSC-height trigger of 60, chosen using a bead-only control. Approximately 10 000 events per sample were collected. Of these, typically over 98% were FITC-positive, using a B1-area threshold of 1×10^3. Negative mCherry values (negative Y2-area below zero, indicative of noise distribution around 0, typically less than 10% of FITC-positive events) were assigned a value of zero. Boxplot measurements shown are the mCherry fluorescence values of the FITC-positive events, with black marker indicating the median, colored bar spanning from the 25th to the 75th percentile, and whiskers extending to extreme data points not considered outliers (using the Matlab boxplot function).

Optimal Loading of Protein onto the Carboxyl Fluorescent Yellow Particles. The carboxyl polystyrene fluorescent yellow particles were centrifuged after the first step of the reaction (see Supplemental Method for detailed synthesis of v-particle) for 15 min at 3000*g* and the supernatant was replaced with tdPP7-mCherry (Figure 2A) or RBD (for v-particle, Figure 2B) in 100 μL of 1x PBS, and incubated on ice with 145 rpm horizontal shaking for 2.5 h while protected from light. The sample was centrifuged for 15 min at 3000*g*, and the supernatant was replaced with 100 μL of 1x PBS, 3 times. The synthesized particle stock was stored at 4 °C, and could be used for approximately 3 weeks. Final fluorescent particle concentration in the particle stock is approximately 1% w/v. One bead particle contains up to 300 000 COOH functional groups and can therefore theoretically bind a maximum of 300 000 protein molecules. We optimized the binding ratio, using 1 bead particle to the following amounts of protein molecules: 0.001x, 0.01x, 0.1x, 0.5x, 1x, 2x, 5x, 10x (x = 300 000 protein molecules). In a Lo-Bind microcentrifuge tube, we combined 0.5 μL of presonicated protein−particle stock with 99.5 μL of 1x PBS and measured by flow cytometry as described above. For tdPP7-mCherry, we did not add any hACE2F (Figure 2A). For RBD, we added a constant amount of 0.34 μg of hACE2F (Figure 2B).

Specificity of V-particle Binding to hACE2F. In a Lo-Bind microcentrifuge tube, we combined 0.5 μL of presonicated v-particle stock or 1% w/v carboxyl polystyrene fluorescent yellow particles, 10 μg of BSA and either 0.05, 0.25, 0.5, or 1 μg of hACE2F (1 μg of hACE2F is equivalent to a RBD/hACE2F ratio of 1:2). Sample volumes were adjusted to 3 μL with 1x PBS. Samples were incubated, diluted, and measured by flow cytometry as described above.

Sensitivity of V-particles to hACE2F. In a Lo-Bind microcentrifuge tube, 0.5 μL of presonicated v-particle stock and 10 μg of BSA were mixed with one of the following amounts of hACE2F: 5 ng, 12.5 ng, 0.05 μg, 0.125 μg, or 0.5 μg hACE2F (RBD/hACE2F ratios of 1:0.01, 1:0.025, 1:0.1, 1:0.25, and 1:1). The volume was adjusted to 3 μL with 1x PBS. Samples were prepared in triplicate. Samples were incubated, diluted, and measured by flow cytometry as described above.

Optimal Time for Binding Reactions. In a Lo-Bind microcentrifuge tube, 0.5 μL of presonicated v-particle stock, 10 μg of BSA, and 1 μg of hACE2F (equivalent to RBD/hACE2F of 1:2) were added, and the volume was adjusted to 3 μL with 1x PBS. The samples were incubated for different amounts of time: 15, 45, 90, 180 min, and 24 h. Samples were prepared in triplicate. Samples were diluted and measured by flow cytometry as described above.

Maximizing Fluorescent Signal Associated with hACE2F binding to V-particle. V-particles were synthesized with carboxyl-particle/RBD ratios of 1:0.001x, 1:0.01x 1:0.1x, 1:0.5x, 1:1x, 1:2x, 1:5x, and 1:10x (x = 300 000 RBD particle = 1.4×10^{-2} pg RBD). In a Lo-Bind microcentrifuge tube, we combined 0.5 μL of presonicated v-particle stock with 10 μg of BSA and 0.34 μg of hACE2F. Total volume was adjusted to 5 μL. Samples were incubated, diluted, and measured by flow cytometry as described above.

Inhibition of V-particle−hACE2F Binding. In a Lo-Bind microcentrifuge tube, 0.5 μL of presonicated 0.5x RBD−v-particle stock (0.5 μL v-particle contains up to 2.8×10^{-12} mol RBD), 10 μg of BSA, and Sybody in one of the following amounts: 0, 34 ng, 0.17, 0.34, 1.7, 3.4 μg (ratio per 0.5 RBD: 0, 1, 10, 100 Sybody inhibitor/2.5 hACE2F) or 0.5 μL of presonicated v-particle stock (0.5 μL v-particle contains 0.6×10^{-11} mol RBD), negative inhibitor protein in one of the following amounts: BSA 0, 5, 10, 20 μg (ratio per 1 RBD: 15, 30, 60 BSA) or GST 0, 0.5, 1, 2 μg (ratio per 1 RBD: 3, 6, 12 GST) was added, and the volume was adjusted to 6 μL with 1x PBS. Next, 1.25 μg of hACE2F (0.5 RBD:2.5 hACE2F) or (1 RBD:2.5 hACE2F) was added to all the samples. Total volume was 13 μL. Samples were incubated, diluted, and measured by flow cytometry as described above.

Selective Binding of the SRNP Granules to the V-particles. SRNP experiments were performed in granule buffer (GB: 750 mM NaCl, 1 mM $MgCl_2$, 10% PEG 4000, in water). Reactions containing 8 μL of GB, 1 μg of tdPP7-mCherry or 1.5 μg of hACE2F (in 1 μL), 0 or 1 μg of slncRNA-PP7bsx14 (in 1 μL), and 0.5 μL of Ribolock RNase Inhibitor (Thermo Fisher) were incubated at room temperature for 1 h. After 1 h, 1 μL from each reaction was deposited on a glass slide, together with 1 μL of presonicated 1% w/v v-particle stock diluted 1:5 in water. A 1 μL control sample of undiluted v-particle stock was also deposited. After 10 min, the samples were sealed with coverslips and imaged using a 100x oil immersion objective on a Nikon Eclipse Ti epifluorescent microscope with iXon Ultra EMCCD camera (Andor) and NIS-Elements software (Nikon), with 585 nm (mCherry) and 490 nm (FITC) excitation using a CooLED PE illumination system (CooLED Ltd.).

■ ASSOCIATED CONTENT

Supporting Information

The Supporting Information is available free of charge at https://pubs.acs.org/doi/10.1021/acssynbio.1c00381.

List of the nucleotide sequences of all proteins and RNA components used in this work; description of methods used for expression and extraction of the proteins used in this work; and a description of v-particle generation (PDF)

■ AUTHOR INFORMATION

Corresponding Author

Roee Amit − *Department of Biotechnology and Food Engineering, Technion—Israel Institute of Technology, Haifa*

https://doi.org/10.1021/acssynbio.1c00381
ACS Synth. Biol. 2022, 11, 1389−1396

32000, Israel; orcid.org/0000-0003-0580-7076; Email: roeeamit@technion.ac.il

Authors

Nanami Kikuchi − *Department of Biotechnology and Food Engineering, Technion—Israel Institute of Technology, Haifa 32000, Israel*

Or Willinger − *Department of Biotechnology and Food Engineering, Technion—Israel Institute of Technology, Haifa 32000, Israel*

Naor Granik − *Department of Biotechnology and Food Engineering, Technion—Israel Institute of Technology, Haifa 32000, Israel*

Reut Gal − *Department of Biotechnology and Food Engineering, Technion—Israel Institute of Technology, Haifa 32000, Israel*

Noa Navon − *Department of Biomedical Engineering and Department of Biotechnology and Food Engineering, Technion—Israel Institute of Technology, Haifa 32000, Israel*

Shanny Ackerman − *Department of Biotechnology and Food Engineering, Technion—Israel Institute of Technology, Haifa 32000, Israel*

Ella Samuel − *Department of Biotechnology and Food Engineering, Technion—Israel Institute of Technology, Haifa 32000, Israel*

Tomer Antman − *Department of Biotechnology and Food Engineering, Technion—Israel Institute of Technology, Haifa 32000, Israel*

Noa Katz − *Department of Biotechnology and Food Engineering, Technion—Israel Institute of Technology, Haifa 32000, Israel*

Sarah Goldberg − *Department of Biotechnology and Food Engineering, Technion—Israel Institute of Technology, Haifa 32000, Israel;* orcid.org/0000-0003-1062-2084

Complete contact information is available at: https://pubs.acs.org/10.1021/acssynbio.1c00381

Author Contributions

N. Kikuchi, O.W., and N.G. are equally contributing first authors. N. Kikuchi, O.W., N.G., S.G., and R.A. conceived the approach and designed the experiments. N. Kikuchi prepared the v-particles and carried out binding experiments. N.G. prepared slncRNA-PP7bsx14 and carried out microscopy experiments. O.W. and S.G. expressed and purified RBD, hACE2F, and tdPP7-mCherry, and assisted with binding experiments. N.N. assisted with RBD secretion and purification. N. Katz assisted with slncRNA-PP7bsx14 design. R.G., N.G., S.G., and S.A. expressed and purified sybodies. S.A., E.S., and T.A. designed Sb#15 and Sb#68 expression vectors. N. Kikuchi, O.W., N.G., S.G., and R.A. prepared the manuscript. All authors have given approval to the final version of the manuscript.

Funding

This research was funded in part by the Zuckerman Fellowship supported at the Technion, and European Union's Horizon 2020 Research and Innovation Programme under grant agreement 851065 (CARBP).

Notes

The authors declare the following competing financial interest(s): N. Kikuchi, O.W., N.G., S.G., and R.A. are inventors on US Provisional Patent Application No. 63/187969 concerning some of the described technologies. N. Katz and R.A. are inventors on US Patent Application 2021/0095296 A1.

■ ACKNOWLEDGMENTS

We thank Omer Yehezkeli, Smadar Shulami, Onit Alalouf, and Moran Bercovici from the Technion for expert advice. N. Kikuchi acknowledges the support of the Zuckerman STEM Leadership program. We thank Integrated DNA Technologies for contributing the gBlocks encoding Sb#15 and Sb#68 to the Technion 2020 iGEM team. We thank the Florian Krammer lab for the plasmid encoding RBD. We thank the Marcus Seeger lab for the plasmid encoding GS4. Special thanks to J. D. Walter for advice regarding sybodies.

■ ABBREVIATIONS

RBD, SARS-CoV-2 Spike receptor-binding domain; hACE2, human angiotensin-converting enzyme 2; tdPP7, tandem-dimer form of bacteriophage PP7 coat protein; hACE2F, fluorescently labeled hACE2 also containing tdPP7; slncRNA-PP7bsx14, synthetic long noncoding RNA harboring 14 binding sites of bacteriophage PP7 coat-protein

■ REFERENCES

(1) Zhu, N.; Zhang, D.; Wang, W.; Li, X.; Yang, B.; Song, J.; Zhao, X.; Huang, B.; Shi, W.; Lu, R.; Niu, P.; Zhan, F.; Ma, X.; Wang, D.; Xu, W.; Wu, G.; Gao, G. F.; Tan, W. A Novel Coronavirus from Patients with Pneumonia in China. *N. Engl. J. Med.* **2020**, *382*, 727.

(2) Zhou, P.; Yang, X.-L.; Wang, X.-G.; Hu, B.; Zhang, L.; Zhang, W.; Si, H.-R.; Zhu, Y.; Li, B.; Huang, C.-L.; Chen, H.-D.; Chen, J.; Luo, Y.; Guo, H.; Jiang, R.-D.; Liu, M.-Q.; Chen, Y.; Shen, X.-R.; Wang, X.; Zheng, X.-S.; Zhao, K.; Chen, Q.-J.; Deng, F.; Liu, L.-L.; Yan, B.; Zhan, F.-X.; Wang, Y.-Y.; Xiao, G.-F.; Shi, Z.-L. A Pneumonia Outbreak Associated with a New Coronavirus of Probable Bat Origin. *Nature* **2020**, *579* (7798), 270−273.

(3) Yan, R.; Zhang, Y.; Li, Y.; Xia, L.; Guo, Y.; Zhou, Q. Structural Basis for the Recognition of SARS-CoV-2 by Full-Length Human ACE2. *Science* **2020**, *367* (6485), 1444−1448.

(4) Wang, Q.; Zhang, Y.; Wu, L.; Niu, S.; Song, C.; Zhang, Z.; Lu, G.; Qiao, C.; Hu, Y.; Yuen, K.-Y.; Wang, Q.; Zhou, H.; Yan, J.; Qi, J. Structural and Functional Basis of SARS-CoV-2 Entry by Using Human ACE2. *Cell* **2020**, *181* (4), 894−904.e9.

(5) Du, L.; Yang, Y.; Zhang, X. Neutralizing Antibodies for the Prevention and Treatment of COVID-19. *Cell. Mol. Immunol.* **2021**, *18* (10), 2293−2306.

(6) Hughes, J.; Rees, S.; Kalindjian, S.; Philpott, K. Principles of Early Drug Discovery. *Br. J. Pharmacol.* **2011**, *162* (6), 1239−1249.

(7) Pushpakom, S.; Iorio, F.; Eyers, P. A.; Escott, K. J.; Hopper, S.; Wells, A.; Doig, A.; Guilliams, T.; Latimer, J.; McNamee, C.; Norris, A.; Sanseau, P.; Cavalla, D.; Pirmohamed, M. Drug Repurposing: Progress, Challenges and Recommendations. *Nat. Rev. Drug Discovery* **2019**, *18* (1), 41−58.

(8) Mercorelli, B.; Palù, G.; Loregian, A. Drug Repurposing for Viral Infectious Diseases: How Far Are We? *Trends Microbiol* **2018**, *26* (10), 865−876.

(9) Galindez, G.; Matschinske, J.; Rose, T. D.; Sadegh, S.; Salgado-Albarrán, M.; Späth, J.; Baumbach, J.; Pauling, J. K. Lessons from the COVID-19 Pandemic for Advancing Computational Drug Repurposing Strategies. *Nat. Comput. Sci.* **2021**, *1* (1), 33−41.

(10) Kuleshov, M. V.; Stein, D. J.; Clarke, D. J. B.; Kropiwnicki, E.; Jagodnik, K. M.; Bartal, A.; Evangelista, J. E.; Hom, J.; Cheng, M.; Bailey, A.; Zhou, A.; Ferguson, L. B.; Lachmann, A.; Ma'ayan, A. The COVID-19 Drug and Gene Set Library. *Patterns* **2020**, *1* (6), 100090.

(11) Nie, J.; Li, Q.; Wu, J.; Zhao, C.; Hao, H.; Liu, H.; Zhang, L.; Nie, L.; Qin, H.; Wang, M.; Lu, Q.; Li, X.; Sun, Q.; Liu, J.; Fan, C.; Huang, W.; Xu, M.; Wang, Y. Quantification of SARS-CoV-2

Neutralizing Antibody by a Pseudotyped Virus-Based Assay. *Nat. Protoc.* **2020**, *15* (11), 3699−3715.
(12) Neerukonda, S. N.; Vassell, R.; Herrup, R.; Liu, S.; Wang, T.; Takeda, K.; Yang, Y.; Lin, T.-L.; Wang, W.; Weiss, C. D. Establishment of a Well-Characterized SARS-CoV-2 Lentiviral Pseudovirus Neutralization Assay Using 293T Cells with Stable Expression of ACE2 and TMPRSS2. *PLoS One* **2021**, *16* (3), No. e0248348.
(13) Contreras-Llano, L. E.; Tan, C. High-Throughput Screening of Biomolecules Using Cell-Free Gene Expression Systems. *Synth. Biol.* **2018**, *3* (1), ysy012.
(14) Medhi, R.; Srinoi, P.; Ngo, N.; Tran, H.-V.; Lee, T. R. Nanoparticle-Based Strategies to Combat COVID-19. *ACS Appl. Nano Mater.* **2020**, *3* (9), 8557−8580.
(15) Norman, M.; Gilboa, T.; Ogata, A. F.; Maley, A. M.; Cohen, L.; Busch, E. L.; Lazarovits, R.; Mao, C.-P.; Cai, Y.; Zhang, J.; Feldman, J. E.; Hauser, B. M.; Caradonna, T. M.; Chen, B.; Schmidt, A. G.; Alter, G.; Charles, R. C.; Ryan, E. T.; Walt, D. R. Ultrasensitive High-Resolution Profiling of Early Seroconversion in Patients with COVID-19. *Nat. Biomed. Eng.* **2020**, *4* (12), 1180−1187.
(16) Dogan, M.; Kozhaya, L.; Placek, L.; Gunter, C.; Yigit, M.; Hardy, R.; Plassmeyer, M.; Coatney, P.; Lillard, K.; Bukhari, Z.; Kleinberg, M.; Hayes, C.; Arditi, M.; Klapper, E.; Merin, N.; Liang, B. T.-T.; Gupta, R.; Alpan, O.; Unutmaz, D. SARS-CoV-2 Specific Antibody and Neutralization Assays Reveal the Wide Range of the Humoral Immune Response to Virus. *Commun. Biol.* **2021**, *4* (1), 1−13.
(17) Baker, M. How Quality Control Could Save Your Science. *Nature* **2016**, *529* (7587), 456−458.
(18) Amanat, F.; Stadlbauer, D.; Strohmeier, S.; Nguyen, T. H. O.; Chromikova, V.; McMahon, M.; Jiang, K.; Arunkumar, G. A.; Jurczyszak, D.; Polanco, J.; Bermudez-Gonzalez, M.; Kleiner, G.; Aydillo, T.; Miorin, L.; Fierer, D. S.; Lugo, L. A.; Kojic, E. M.; Stoever, J.; Liu, S. T. H.; Cunningham-Rundles, C.; Felgner, P. L.; Moran, T.; García-Sastre, A.; Caplivski, D.; Cheng, A. C.; Kedzierska, K.; Vapalahti, O.; Hepojoki, J. M.; Simon, V.; Krammer, F. A Serological Assay to Detect SARS-CoV-2 Seroconversion in Humans. *Nat. Med.* **2020**, *26*, 1033−1036.
(19) Tate, J.; Ward, G. Interferences in Immunoassay. *Clin. Biochem. Rev.* **2004**, *25* (2), 105−120.
(20) Walter, J. D.; Hutter, C. A. J.; Zimmermann, I.; Wyss, M.; Egloff, P.; Sorgenfrei, M.; Hürlimann, L. M.; Gonda, I.; Meier, G.; Remm, S.; Thavarasah, S.; Plattet, P.; Seeger, M. A. Sybodies Targeting the SARS-CoV-2 Receptor-Binding Domain. *bioRxiv* (Biochemistry) 2020.04.16.045419v2, **2020**, DOI: 10.1101/2020.04.16.045419.
(21) Lin, Y.; Protter, D. S. W.; Rosen, M. K.; Parker, R. Formation and Maturation of Phase-Separated Liquid Droplets by RNA-Binding Proteins. *Mol. Cell* **2015**, *60* (2), 208−219.
(22) Nakamura, H.; Lee, A. A.; Afshar, A. S.; Watanabe, S.; Rho, E.; Razavi, S.; Suarez, A.; Lin, Y.-C.; Tanigawa, M.; Huang, B.; DeRose, R.; Bobb, D.; Hong, W.; Gabelli, S. B.; Goutsias, J.; Inoue, T. Intracellular Production of Hydrogels and Synthetic RNA Granules by Multivalent Molecular Interactions. *Nat. Mater.* **2018**, *17* (1), 79−89.
(23) Han, T. W.; Kato, M.; Xie, S.; Wu, L. C.; Mirzaei, H.; Pei, J.; Chen, M.; Xie, Y.; Allen, J.; Xiao, G.; McKnight, S. L. Cell-Free Formation of RNA Granules: Bound RNAs Identify Features and Components of Cellular Assemblies. *Cell* **2012**, *149* (4), 768−779.
(24) Granik, N.; Katz, N.; Goldberg, S.; Amit, R. Formation of Synthetic RNP Granules Using Engineered Phage-Coat-Protein - RNA Complexes*bioRxiv* (Biopysics) 682518v3, **2021**, DOI: 10.1101/682518.
(25) Daly, J. L.; Simonetti, B.; Klein, K.; Chen, K.-E.; Williamson, M. K.; Antón-Plágaro, C.; Shoemark, D. K.; Simón-Gracia, L.; Bauer, M.; Hollandi, R.; Greber, U. F.; Horvath, P.; Sessions, R. B.; Helenius, A.; Hiscox, J. A.; Teesalu, T.; Matthews, D. A.; Davidson, A. D.; Collins, B. M.; Cullen, P. J.; Yamauchi, Y. Neuropilin-1 Is a Host Factor for SARS-CoV-2 Infection. *Science* **2020**, *370* (6518), 861−865.
(26) Li, F. Structure, Function, and Evolution of Coronavirus Spike Proteins. *Annu. Rev. Virol.* **2016**, *3* (1), 237−261.

https://doi.org/10.1021/acssynbio.1c00381
ACS Synth. Biol. 2022, 11, 1389−1396